Boosting electrocatalytic oxygen evolution activity of bimetallic CoFe selenite by exposing the specific crystal facets

Zheng-Han Guo, Ling-Li Zhou, Dong-Sheng Pan, Sai Huang, Jin-Kun, Li and Jun-Ling Song*

International Joint Research Center for Photoresponsive Molecules and Materials, School of Chemical and Material Engineering, Jiangnan University, Lihu Street 1800, Wuxi 214122, China.

*Corresponding Author. E-mail: s070054@e.ntu.edu.sg

Content

Materials

All reagents were used as purchased without further purification. Co $(OH)_2$ (98%, Macklin), $Fe(NO_3)_3 \cdot 9H_2O$ (98%, Adamas), SeO_2 (99%, Macklin), $NH_3 \cdot H_2O$ (35%, Sinopharm Chemical), KOH (99%, Sinopharm Chemical), IrO_2 (99.9%, Adamas), Pt/C (20%, Macklin), Nafion (5 wt%, Alfa-Aesar), ethanol (AR, Sinopharm Chemical).

Physical Characterization

Powder X-ray diffraction (PXRD) patterns were collected recorded by Bruker D8 instrument with Cu-Kα radiation (λ = 1.5406 Å); the spectra were recorded in the 2θ range of 5° to 50°. The morphologies were characterized by a Hitachi S4800 microscope, scanning electron microscope (SEM, SU8010), NT-MDT Prima scanning probe microscope, transmission electron microscope (TEM, Joel 2100F) and high-resolution TEM (Tecnai F 20). IR spectra were measured using a Fourier transform infrared spectrometer (FT-IR, Nicolet 6700). XPS measurements were performed on a Thermo ESCALAB 250XI XPS Scanning Microprobe. Thermogravimetric (TG, 1100SF) analyses were measured with a heating rate of 10 °C min^{-1} between 30 and 900 °C under N_2 atmosphere. N_2 adsorption-desorption isotherms were enforced by the Brunauer-Emmett-Teller (BET, 2020 HD88). The oxygen concentrations were conducted using gas chromatography (GC9790).

Electrochemical performance test

All electrochemical tests were carried out in a three-electrode system using a CHI760E electrochemical work station (Shanghai Chenhua, China). A carbon rod and an Hg/HgO electrod were used as the counter electrode, reference electrode and glassy carbon electrode modified with the corresponding catalysts was used as working electrode (surface area = 0.07cm^2). 6 μL as-prepared inks (5 g/L) were dropped onto the surface of the glassy carbon electrode (GC) and then dried under a fume hood for a few minutes. 5 mg of the above catalyst powders was dispersed in a mixed water and ethanol (1:1, v/v) solution 1.0 mL), respectively, and then 10 μL of Nafion solution (5.0 wt %) was added. Before the electrochemical tests, 1 M KOH solution was bubbled by oxygen to reach the H_2O/O_2 equilibrium at 1.23 V vs. reversible hydrogen electrode (RHE) at room temperature. Meanwhile, before the electrochemical OER performance was tested, the electrode was pretreated via cyclic voltammetry (CV) scans at 100 mV/s to reach a stable state. The potentials measured were converted to the reversible hydrogen electrode (RHE) based on the equation $E_{RHE} = E_{Hg/HgO} + 0.059\ pH + 0.098$ V. Electrochemical impedance spectroscopy (EIS) measurements were recorded in the frequency range of 10^5–0.1 Hz with an amplitude of 5 mV under open-circuit potential. The double-layer capacitance (C_{dl}) of the sample was measured by cyclic voltammetry. Capacitive current densities were determined in the potential region 0.14 to 0.26 V versus Hg/HgO at the scan rates 20, 40, 60, 80, and 100 mV s^{-1}. The overall water splitting performance of the sample as both anode and cathode catalysts was constructed under 1.0 M KOH electrolyte.

Calculation Method

The values of mass activity (A g^{-1}) were calculated from the catalyst loading m (0.43 mg cm_{geo}^{-2}) and the measured current density j (mA cm_{geo}^{-2}) at η = 0.35 V:

$$\text{mass activity} = \frac{j}{m}$$

The values of TOF were calculated by assuming that every metal atom is involved in the catalysis (lower TOF limits were calculated):

$$\text{TOF} = \frac{j \cdot S_{\text{geo}}}{4F \cdot n}$$

Here, j (mA cm_{geo}^{-2}) is the measured current density at η = 0.35 V, S_{geo} (0.07 cm^2) is the surface area of glassy carbon disk, the number 4 means four electrons per mole of O_2, F is Faraday's constant (96485.3 C mol^{-1}), and n is the moles of the metal atom on the electrode calculated from m and the molecular weight of the coated catalysts.

The turnover frequency (TOF) of the catalyst for OER is defined as TOF = $n_{O2}/n_{cat}/t$ where n_{O2} is the amount of oxygen (mol) produced, $n$cat is the amount of catalytic active centers in the catalyst (mol) and t is the electrolysis time (s).

Details concerning the calculation of mass activity, turnover frequency (TOF) and the Faraday efficiency for OER are shown below.

When the electrolysis current is all used for OER,

$$\text{TOF}_{\text{theoretical}} = J/(4 \times F \times m/\text{M})$$

Where J is the current density (mA cm^{-2}) at a given overpotential, F is the faraday constant (96485 C mol^{-1}), m is the mass loading of the catalyst (mg cm^{-2}), and M is the molecular weight of the catalyst unified with one active center per formula unit.

The Faraday efficiency for OER (F_{OER}) is calculated by

F_{OER} = TOF / TOF $_{theoretical}$ × 100%

The obtained gas chromatography peak areas of O_2 and N_2 in the electrolytic cell are:

	0 min	5 min	10 min	15 min	20 min
O_2	657445.3	674461.3	691996.8	708595.5	725006.7
N_2	1943103.8	2001695.9	2054479.8	2095039.7	2163431.7
H_2	0	20080.4	23911.9	27956.5	30154.3

Giving n_{O2} = O_2 concentration (%) × head space volume / (22.4 × 278 / 273) = (17016/ 2993805) × 40 / 1000 / 22.81 mol = 9.97 × 10^{-6} mol. Because n_{cat} = mass loading (mg) / molecular weight / 1000 = 0.04 / (524/2) / 1000 =1.53 × 10^{-7} mol, TOF = 9.97 × 10^{-6} / 1.53 × 10^{-7} / 300 = 0.217 s^{-1}.

Considering all Co ions in NC_4FS-350 (569 g mol^{-1}) as catalytic centers.

TOF $_{theoretical}$ = 10.0 / (4 × 96485 × (5×6/1000) / 524/2) = 0.226 s^{-1} for NC_4FS-350 at 10.0 mA cm^{-2}.

F_{OER} = 0.217 s^{-1} / 0.226 s^{-1} × 100 % = 96.0 %

Table S1. The N content (weight ratio) elemental analysis of NC_4FS-350 (this work) and NC4FS-350.

Catalyst	N %
NC_4FS-350	0.7
NC4FS-350	0.77

Table S2. Comparison of OER activities for the as-prepared electrocatalysts in this study in 1.0 M KOH solution.

Catalyst	Mass activity at η = 0.35 V (A g^{-1})	Onset overpotential (V vs RHE)	TOF at η = 0.35 V (s^{-1})	Tafel slope (mV dec^{-1})
IrO_2	55.95	265	0.033	86.6
NC_4FS	77.45	243	0.115	87.2
NC_4FS-300	78.20	220	0.109	71.8
NC_4FS-350	234.02	199	0.318	56.1
NC_4FS-400	122.68	218	0.149	68.6

Table S3. The electrochemical impedance at Open Circuit Potential in this work.

Catalyst	Charge transfer resistance (R_{ct})	electrolyte resistance (R_s)
IrO_2	3.297	7.453
NC_4FS	2.998	6.551
NC_4FS -300	3.407	5.691
NC_4FS -350	2.373	6.559
NC_4FS -400	2.735	6.591

Table S4. Comparison of the OER performance of NC_4FS-350 with reported catalysts in alkaline solution (1.0 M KOH).

Catalyst	Substrate	η@10 mA.cm^{-2} (mV)	Tafel slope (mV dec^{-1})	Reference
NC_4FS-350	**GC**	**235**	**56.1**	**This work**

NC4FS-350	GC	288	62.3	Journal of Power Sources 483 (2021) 229196.
$NiFe_2O_4$-HNP/CNTs	GC	260	40	Catal. Sci. Technol., 2020, 10, 6970-6976.
KCFS	GC	274	45.6	Chemical Engineering Journal 399 (2020) 125799.
Ni_1Fe_1SeO	GC	257	34	Applied Catalysis B: Environmental 284 (2021) 119758.
Co_3O_4-MoS_2	NF	298	46	Journal of Alloys and Compounds 853 (2021) 156946.
Co-OH-HPi	GC	290	82	ACS Sustainable Chem. Eng. 2019, 7, 3083−3091.
$CoMoP_2$	GC	270	51	J. Mater. Chem. A, 2020, 8, 2001-2007.
Ni-$C_{500\text{-}20}$	CP	353	97	Applied Surface Science 530 (2020) 147192.
NCoBPi-PVP-450	GC	276	55.8	ACS Sustainable Chem. Eng. 2019, 7, 13981-13988.
FeCoMo-Se	CC	264	33	J. Mater. Chem. A, 2020, 8, 7925-7934.
β-$Ni(OH)_2$/FGS	CC	290	40.2	Energy Storage Materials 32 (2020) 272-280.
Fe_2O_3−Mn_2O_3	NF	350	70	ACS Appl. Nano Mater. 2020, 3, 9889-9898.
LFNOSe-III	GC	287	87	ACS Appl. Mater. Interfaces 2020, 12, 41259-41268.
$C_6H_6CoN_2O_4$	CC	215	54	Inorg. Chem. 2020, 59, 12252-12262.
Co-$MoS_{1+X}Se_{1+Y}$	GC	280	71	Applied Surface Science 513 (2020) 145828.
CoPO@C/NF-3	NF	293	111.4	Journal of Energy Chemistry 52 (2021) 139-146.
SyA-Co_2Fe-ST	GC	254	50	ChemSusChem 2020, 13, 1-8.

Table S5. Comparison of the performance of NC*x*FS obtained by different preparation methods.

Catalyst	CoFe ratio	η@10 mA.cm^{-2} (mV)	Tafel slope (mV dec^{-1})	Reference
NC_4FS	4:1	287	87.2	**This work**
NC4FS	4:1	318	60.3	J. Power. Sources. 483 (2021) 229196.

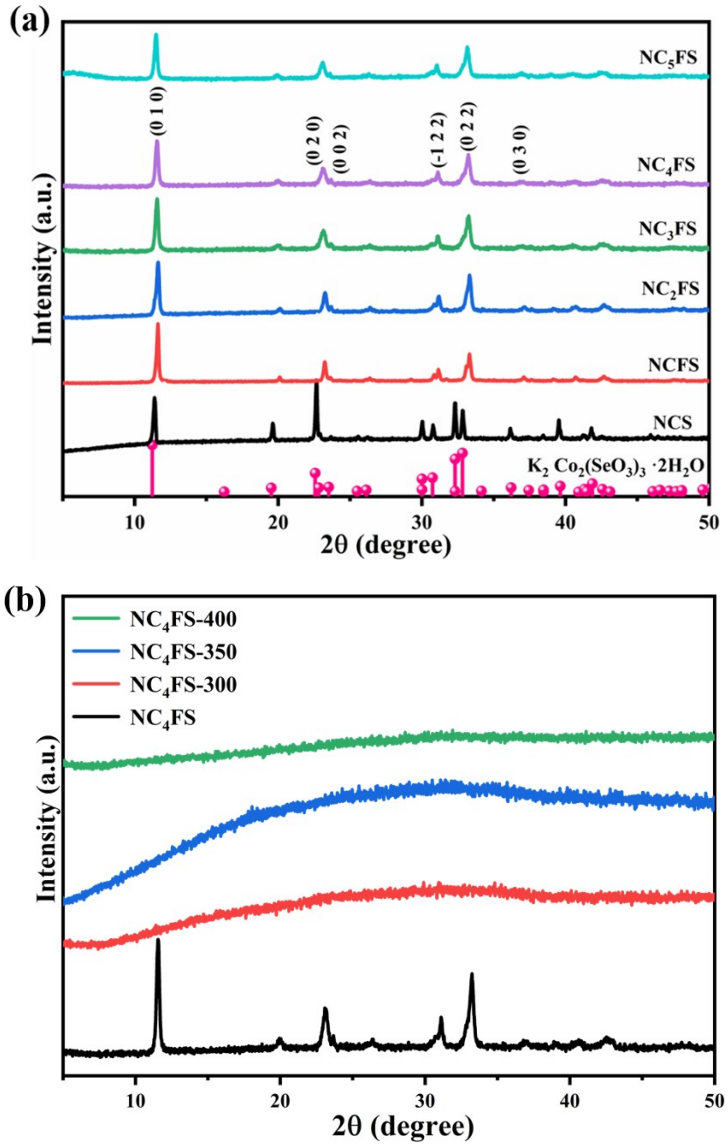

Fig. S1. XRD of (a) NCS and NC_xFS (x = 1, 2, 3, 4 and 5) and (b) NC_4FS-T (T = 300, 350 and 400 ℃).

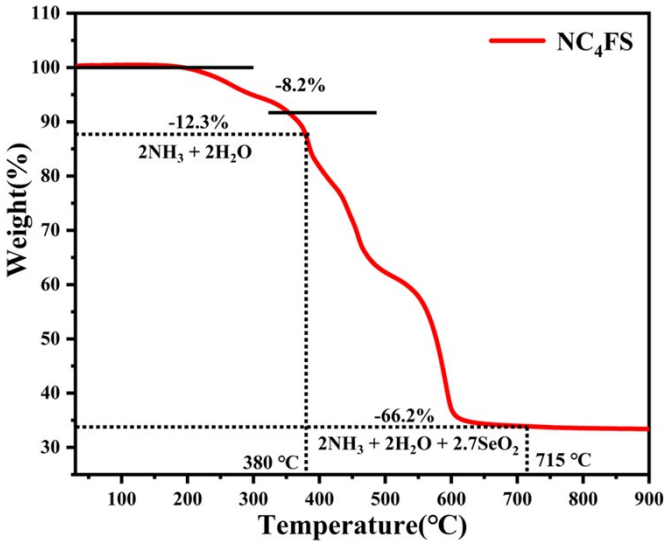

Fig. S2. TGA of NC_4FS.

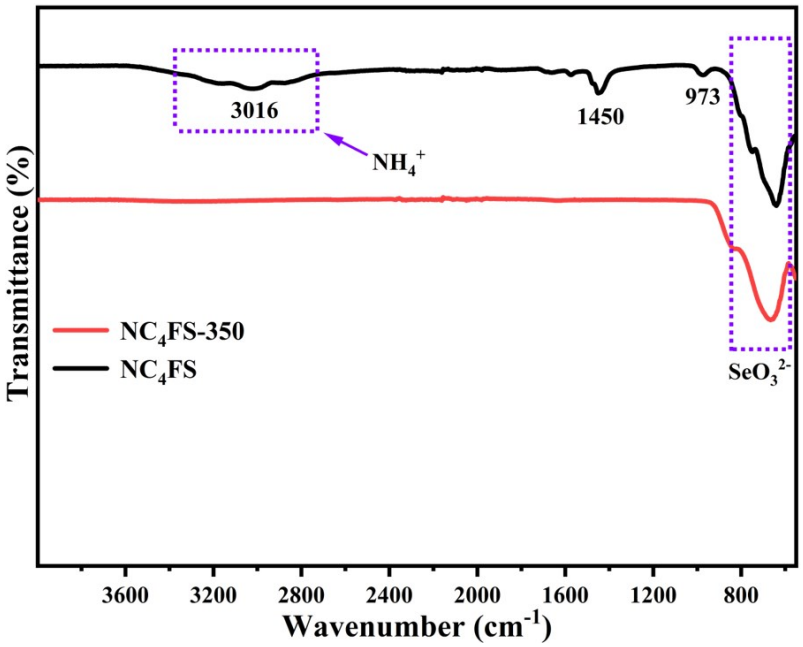

Fig. S3. FT-IR of NC_4FS and NC_4FS-350.

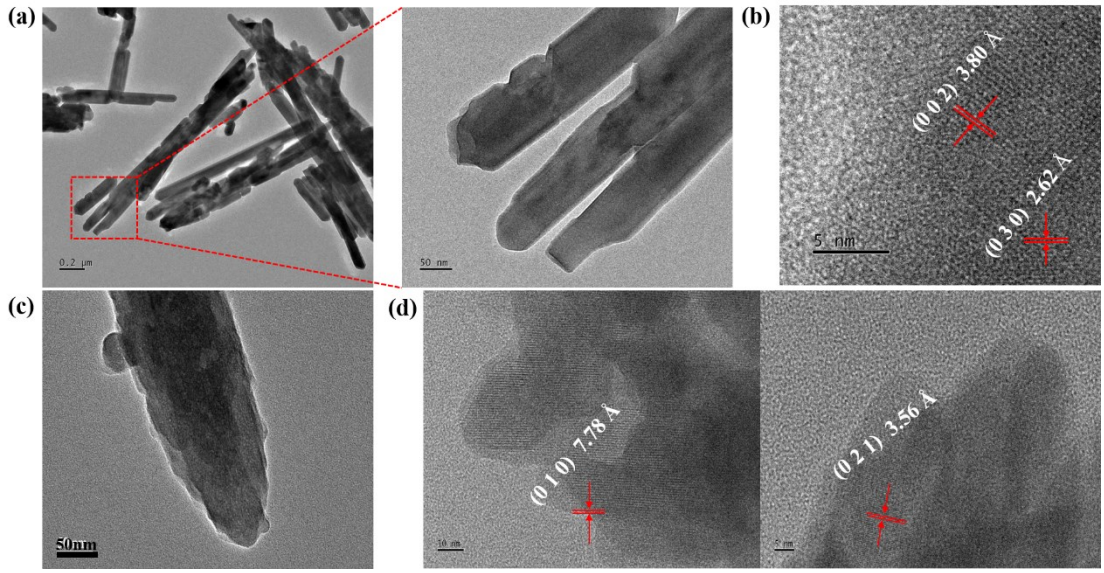

Fig. S4. TEM of (a) NC_4FS in this work and corresponding (b) HR-TEM;

(c) NC4FS in our previous report and corresponding (d) HR-TEM.

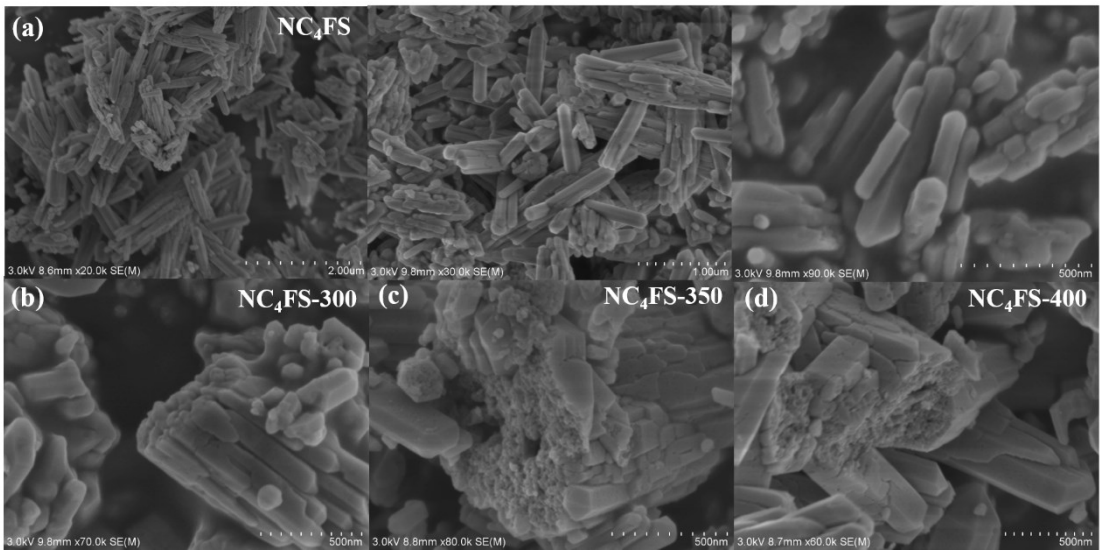

Fig. S5. SEM of (a) NC_4FS, (b) NC_4FS-300, (c) NC_4FS-350 and (d) NC_4FS-400.

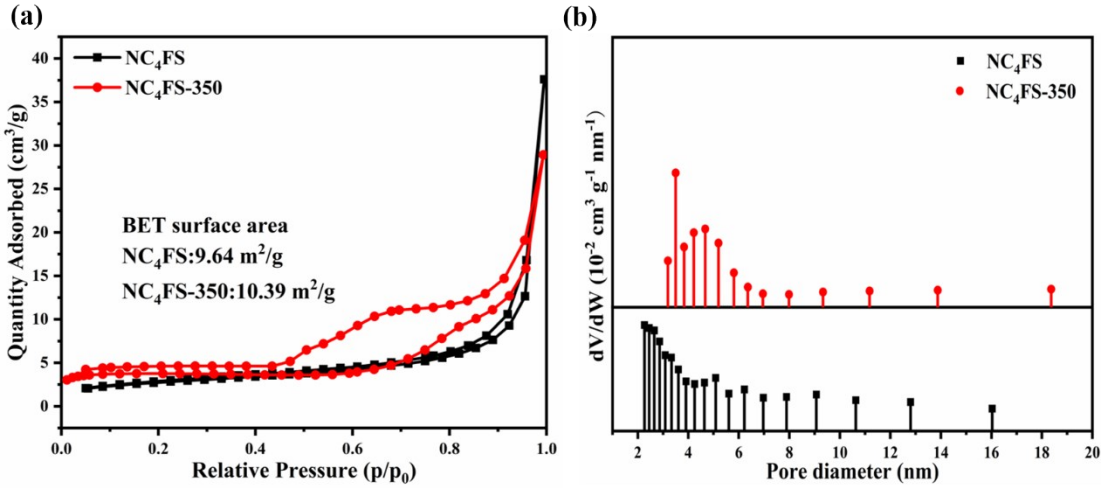

Fig. S6. N_2 adsorption-desorption curve and pore size distribution curve of NC_4FS and NC_4FS-350.

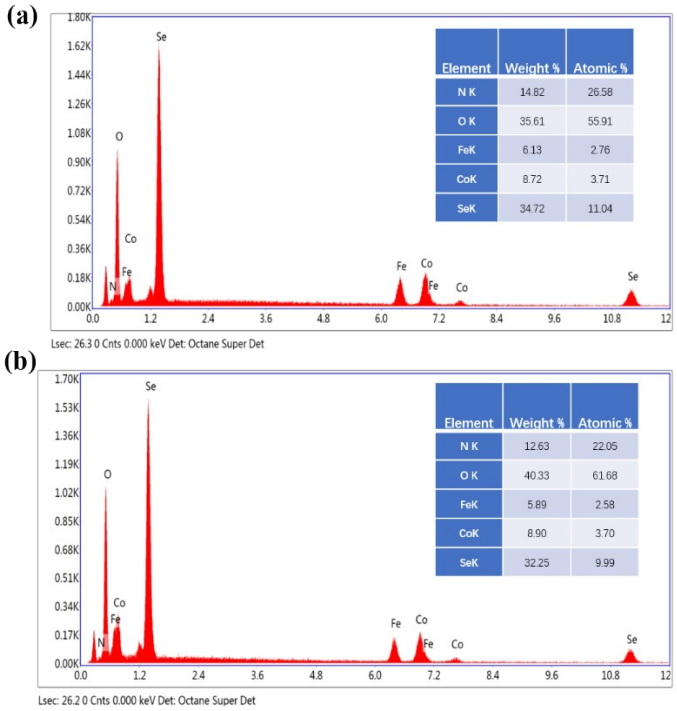

Fig. S7. The EDX patterns of NC_4FS (a) and NC_4FS-350 (b).

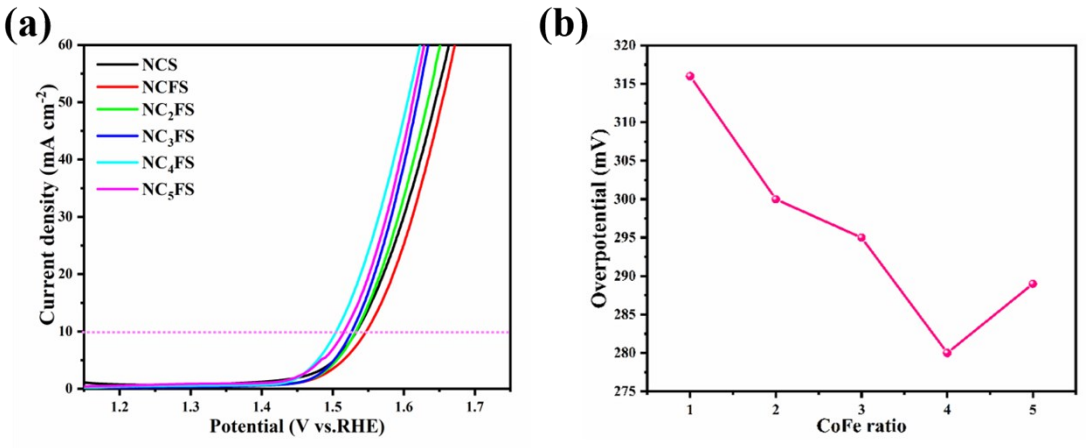

Fig. S8. (a) The LSV curves of NCS, NCFS, NC_2FS, NC_3FS, NC_4FS and NC_5FS; (b) The overpotential of different CoFe ratio at current density of 10 mA cm^{-2}.

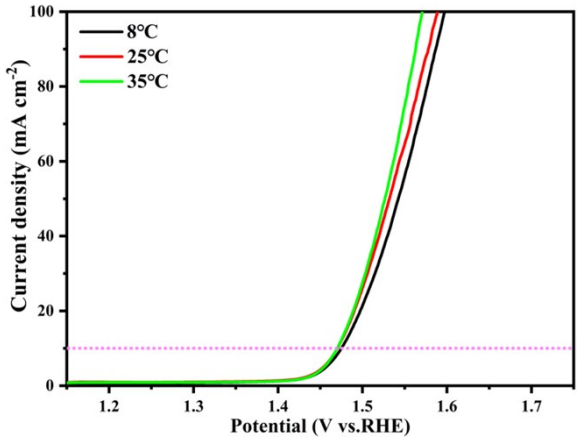

Fig. S9. The LSV curves of NC_4FS-350 at different temperatures.

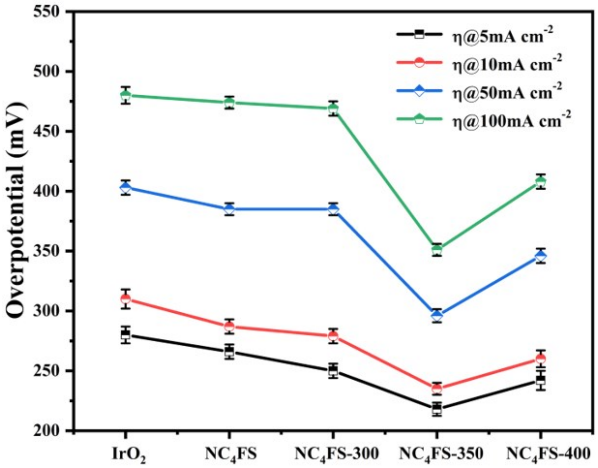

Fig. S10. Comparison of overpotential at different current density of IrO_2, NC_4FS, NC_4FS-300, NC_4FS-350 and NC_4FS-400.

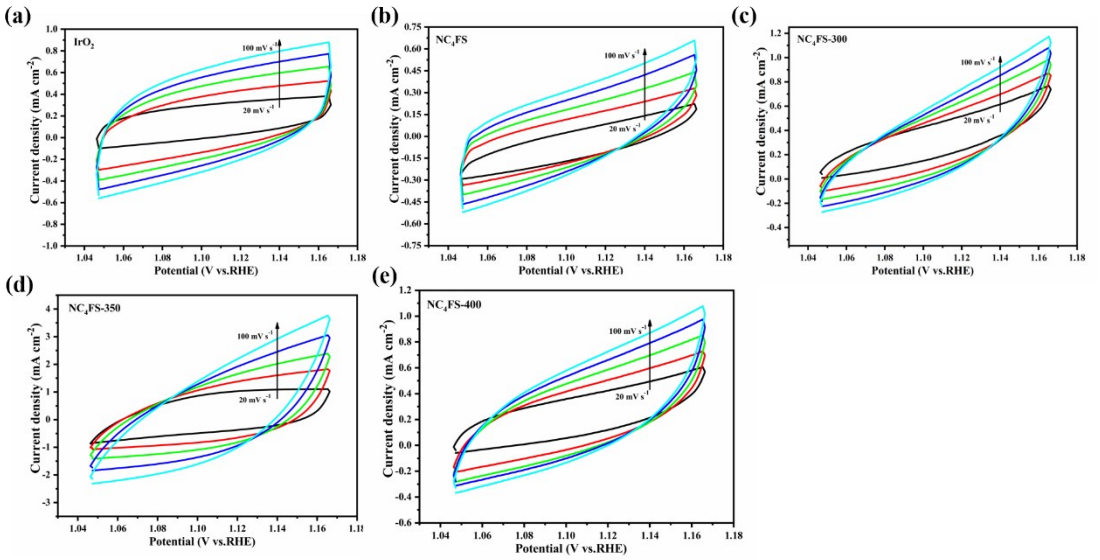

Fig. S11. Cyclic voltammograms of (a) IrO_2, (b) NC_4FS; (c) NC_4FS-300; (d) NC_4FS-350 and (e) NC_4FS-400 at different scan rates from 20 to 100 mV s^{-1}.

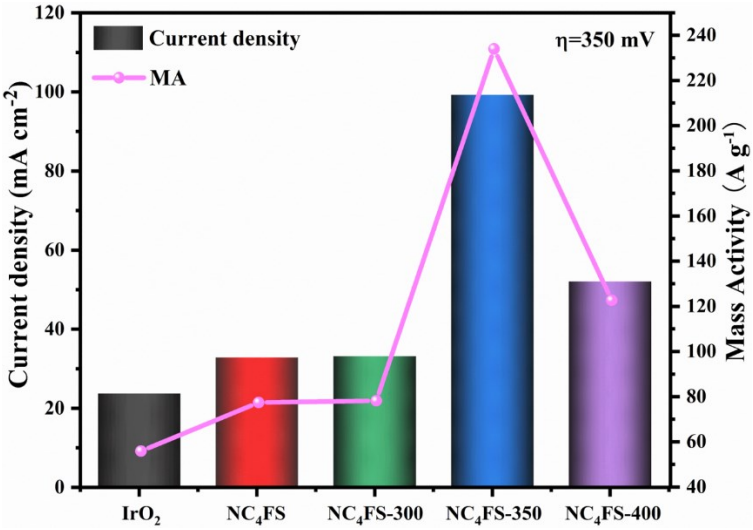

Fig. S12. The current density and Mass activity (MA) of IrO_2, NC_4FS, NC_4FS-300, NC_4FS-350 and NC_4FS-400.

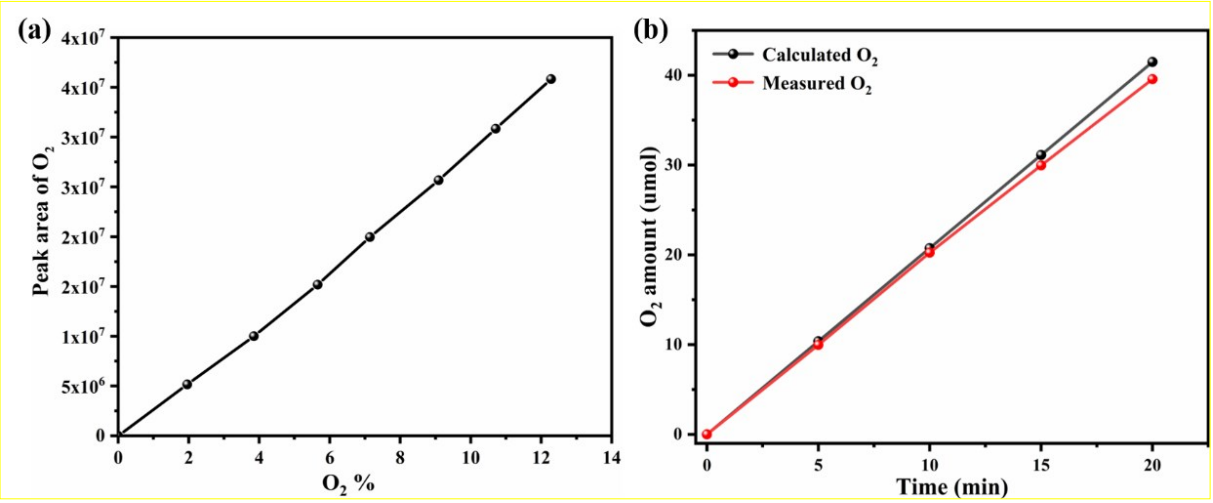

Fig. S13. (a) A linear relationship between seven calibrated O_2 concentrations and their gas chromatography peak areas was obtained, (b) the amount of O_2 theoretically calculated and experimentally measured versus time for the OER of NC_4FS-350.

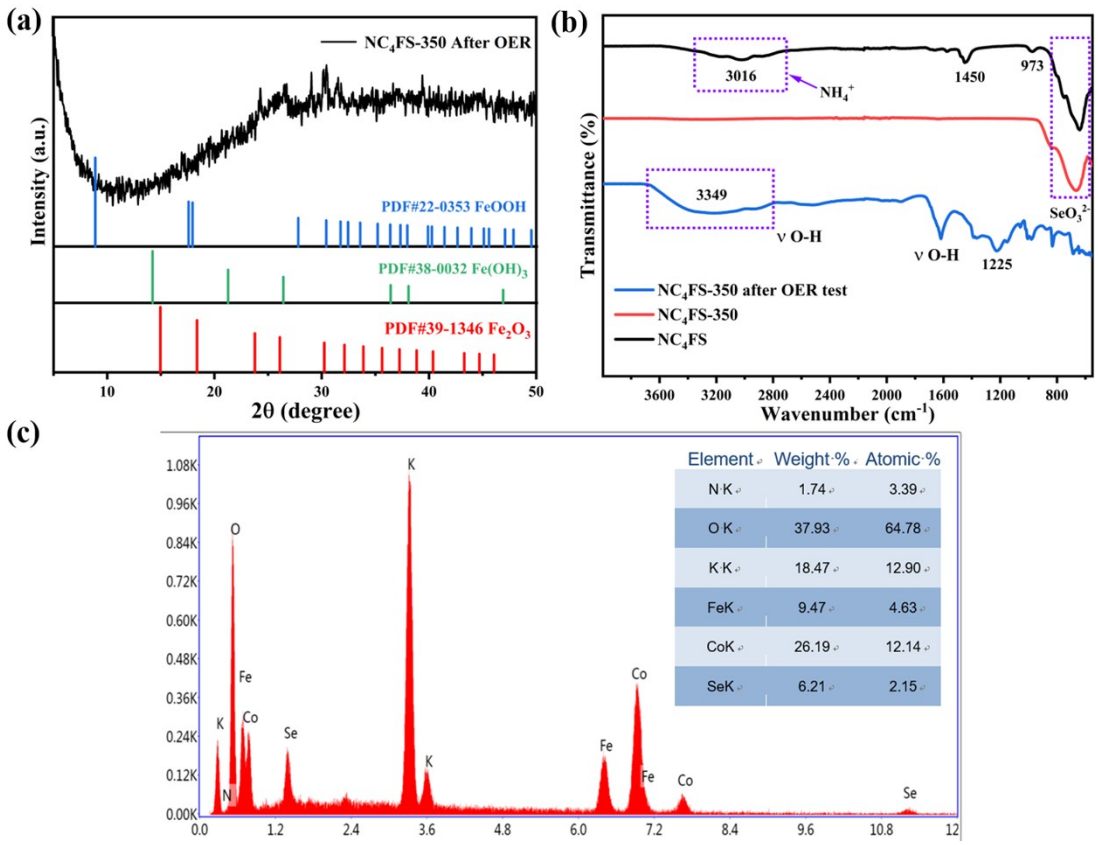

Fig. S14. (a) The XRD patterns, (b) FT-IR spectra and (c) EDX pattern of NC_4FS-350

after OER test.

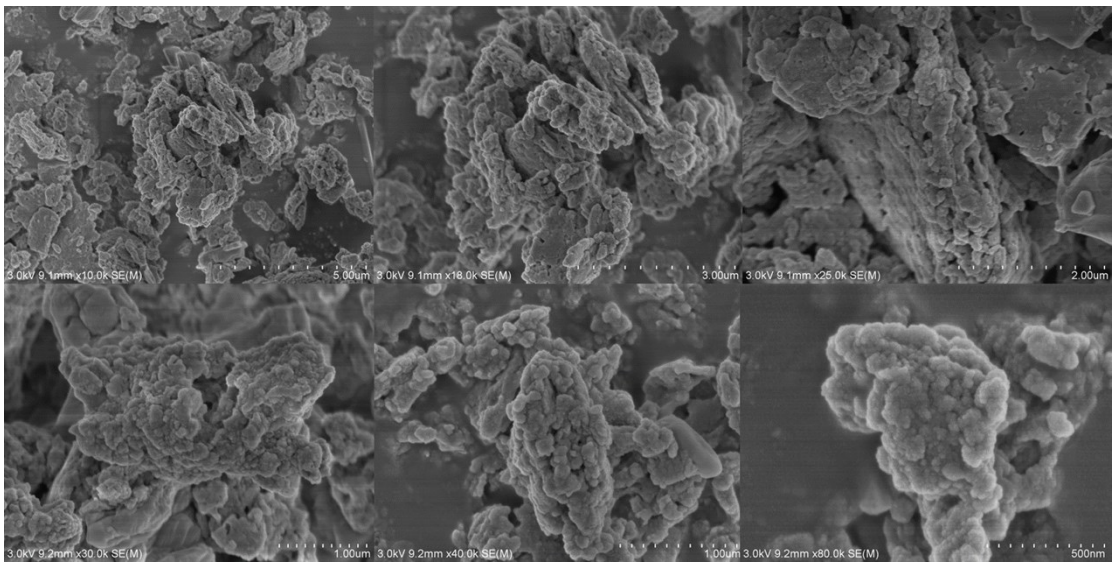

Fig. S15. SEM images of the NC_4FS-350 after OER test.

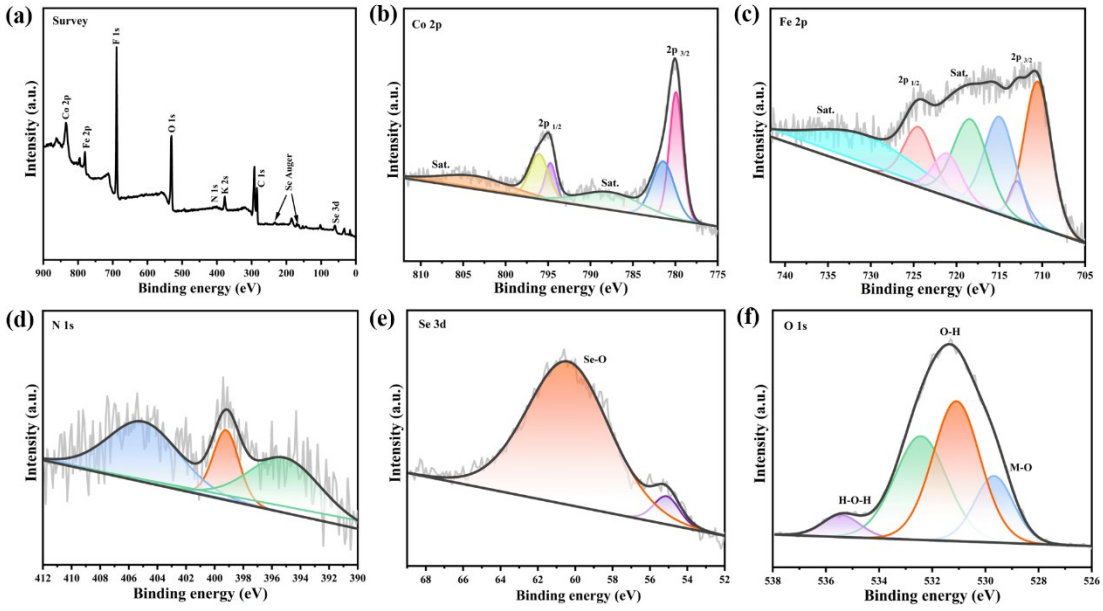

Fig. S16. The XPS spectra of the NC_4FS-350 after OER test. (a) survey, (b) Co 2p, (c) Fe 3d, (d) N 1s, (e) Se 3d and (f) O 1s.

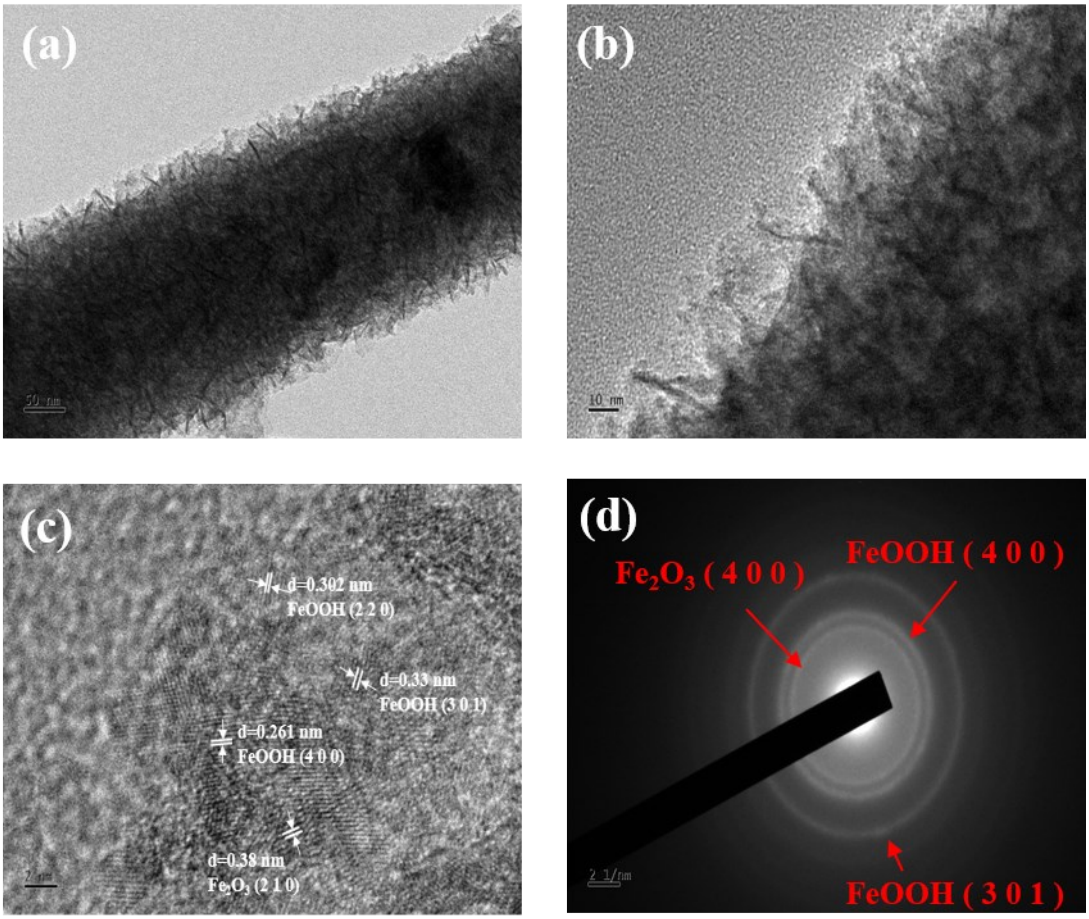

Fig. S17. (a)TEM, (b) HRTEM and (c) SAED pattern of NC_4FS-350 after OER test.

Note: After the OER test, it can be seen from the TEM image that the surface of the NC_4FS-350 has a sheet-like morphology, which can be attributed to the oxide (oxyhydroxide) species. HRTEM further reveals the phase transition occurs after OER test, moreover, d = 0.302, 0.33, 0.261, 0.38 nm can be attributed to (2 2 0) (3 0 1) (4 0 0) crystal planes of FeOOH and (2 1 0) crystal planes of Fe_2O_3, respectively. Tree diffracted rings could be seen for NC_4FS-350 after OER test, further suggesting that the in-situ formation of hydroxide or oxyhydroxide during OER process.

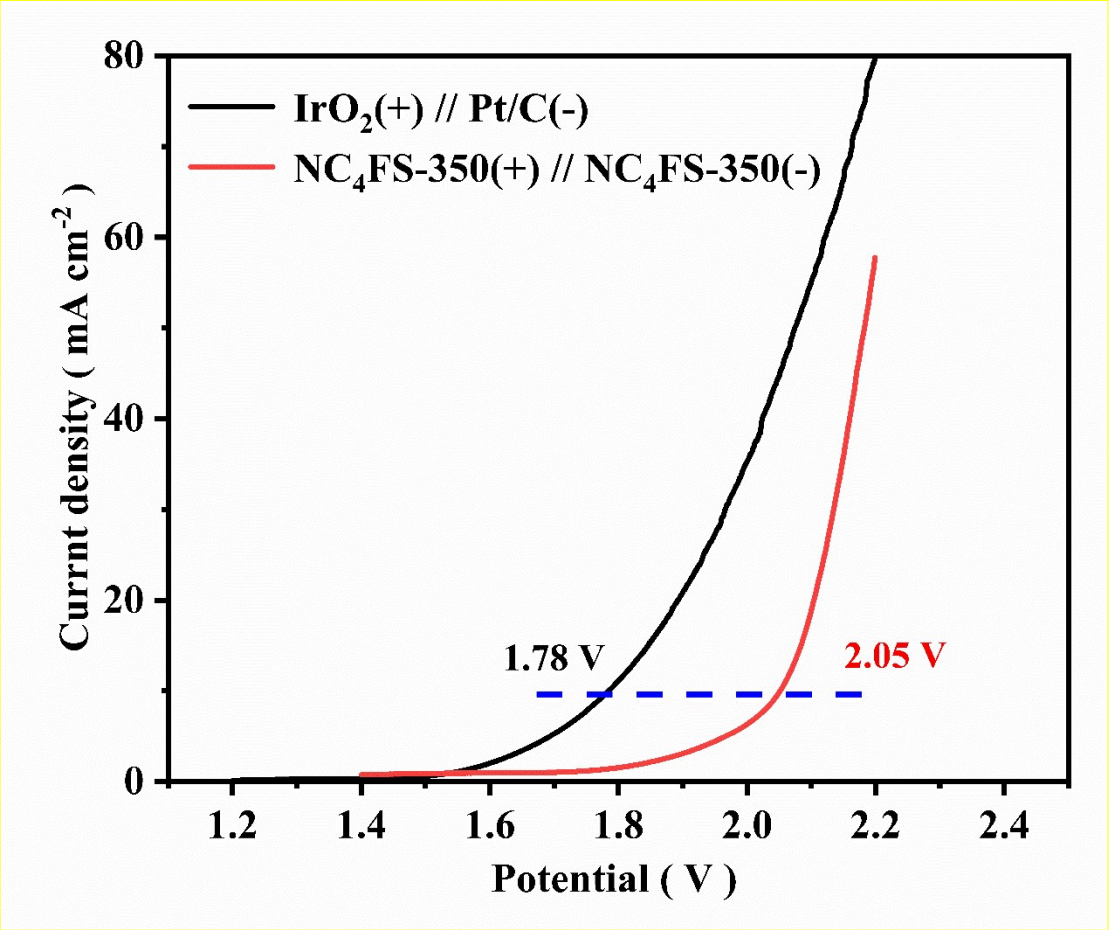

Fig. S18. Overall water splitting performance of NC_4FS-350 as both the anode and cathode (NC_4FS-350 (+)//NC_4FS-350 (-)), and Pt/C(+)//IrO_2(-) electrolyzers in alkaline. solution, sweep rate: 5 mV s^{-1} in 1.0 M KOH.

Note: As shown in **Fig S18**, the potential of overall water splitting at a current density of 10 mA cm^{-2} for NC_4FS-350 (+)//NC_4FS-350 (-) and IrO_2 (+) //Pt/C (-) are 2.05 V and 1.78 V, respectively. NC_4FS-350 as a bifunctional catalyst for overall water splitting has a high voltage, which may be due to its low HER activity.